Vol. 47 — N° 3 09 23 p. 579–594

GEOSTANDARDS and GEOANALYTICAL RESEARCH

A Reappraisal of the $^{40}Ar/^{38}Ar$ Dating Technique via Irradiation with γ-Rays

Jens **Hopp*** , Manfred **Vogt**, Winfried H. **Schwarz** and Mario **Trieloff**

Institut für Geowissenschaften, Klaus-Tschira-Labor für Kosmochemie, Universität Heidelberg, Im Neuenheimer Feld 234-236, D-69120, Heidelberg, Germany

* Corresponding author. e-mail: jens.hopp@geow.uni-heidelberg.de

In a reconnaissance study, we investigated the potential of γ-ray induced production of $^{38}Ar_K$ from ^{39}K for geochronological applications. For this purpose, various age monitors commonly in use for the established $^{40}Ar/^{39}Ar$-method were co-irradiated for 60 h at 17.6 MeV maximum energy in the ELBE facility, Dresden-Rossendorf, Germany. Because the available energy was low, total production of $^{38}Ar_K$ was depressed, leading to low J_{38}-values of (2.1–4.1) × 10^{-6} and hence resulted in only minor ^{38}Ar excess when compared with atmospheric $^{38}Ar/^{36}Ar$ ratios. In spite of these restrictions, ages of younger monitors could be reproduced within error, whereas older age reference materials showed discrepancies due to the low production rate. We observed Ca-derived contributions on ^{36}Ar in analysed CaF_2 reference materials, and calculated a limit for Ca-interference on $^{38}Ar_{Ca}$ of $(^{38}Ar/^{36}Ar)_{Ca} = 0.07 \pm 0.03$ (1*s*). In addition, we investigated a potential recoil redistribution of ^{38}Ar by stepwise heating experiments, but could not quantify this further because of concurring processes. More work at higher photon energies is necessary to resolve other open issues, in particular the potential of utilising $^{40}Ar/^{37}Ar$ ratios for age determination and the possibility of ^{42}Ar production from ^{44}Ca, which would allow correction for Ca-interference reactions on other Ar isotopes. This would be a pre-requisite for dating extra-terrestrial rocks.

Keywords: geochronology, γ-irradiation, $^{40}Ar/^{39}Ar$ dating, age spectra, isochrons.

Received 30 Sep 22 – Accepted 01 Feb 23

^{40}K is a long-lived isotope that decays to ^{40}Ar and ^{40}Ca with a half-life of *ca.* 1.25 Ga. It forms the basis of successful dating methods, the conventional K-Ar method which was already developed about 80 years ago, the $^{40}Ar/^{39}Ar$ dating method developed in the 1960s (Merrihue and Turner 1966) and the K/Ca-method that is currently advancing (e.g., Hogmalm *et al.* 2017). Mitchell (1972) published a study on the geochronological potential of another method – the $^{40}Ar/^{38}Ar$ method – that is based on γ-irradiation of mineral samples. He exploited the main reaction of $^{39}K(\gamma,n)^{38}K(\beta^+, t_{1/2} = 7.7\ min)^{38}Ar$ for calculating ages analogous to the established $^{40}Ar/^{39}Ar$ dating method. For this purpose, four mineral reference materials in use at that time were irradiated for 130 hours with γ-rays produced at the Stanford Linear Accelerator (SLAC) at a maximum energy of 35 MeV. For age calculation, one needs to quantify the production of $^{38}Ar_K$ during this irradiation. In order to avoid use of absolute concentrations it is common practice to choose one reference material of known age and to calculate from measured reference $^{40}Ar^*/^{38}Ar_K$ ratios the proportionality constant (J_{38}-value) necessary for determining the age of unknown samples. This J_{38}-value is calculated from the standard age t_{St} and measured standard $^{40}Ar^*/^{38}Ar_K$-ratios as $J_{38} = \left(e^{\lambda t_{St}} - 1\right) / \left(\frac{^{40}Ar^*}{^{38}Ar_K}\right)$. Note, that this is equivalent to the $^{40}Ar/^{39}Ar$ method including the range of suitable *J*-values. J_{38}-values were in good agreement for each reference material included in the irradiation of Mitchell (1972) and demonstrated the general feasibility of this method for geochronological applications. However, with the continuous success of the $^{40}Ar/^{39}Ar$-method, which utilises neutron irradiation to transform ^{39}K into ^{39}Ar, the γ-method fell into oblivion. A major reason for this development is the difficulty in correcting for interference reactions from Ca isotopes and, at least partially, the low number of potential irradiation facilities. Another reason is the

doi: 10.1111/ggr.12489

natural occurrence of stable, trapped ^{38}Ar in minerals that requires a correction. Several reasons, however, argue for a reconnaissance study. First, Mitchell (1972) published no data on the impact of Ca interference reactions. Second, his age reference materials are out of use and a re-investigation could be based on modern RMs. Third, the neutron-irradiation method causes significant recoil effects of produced ^{39}Ar, which is problematic for small grain sizes below ~ 50 μm (e.g., biotite: Paine *et al.* 2006; feldspar: Jourdan *et al.* 2007, Jourdan and Renne 2013). Hence, an important motivation would be to check if γ-ray irradiation induces a smaller recoil redistribution. A further advantage could be the lower radioactivity produced during the irradiation process, which might allow for a safer handling of the samples. Finally, the availability of reactors for neutron irradiation may be more limited in future, depending on national political decisions, whereas the development of γ-ray facilities for radiosurgery with ever higher energies is still on the rise (devices with energies of 15 MeV are commercially available). In future, this may also allow hosting an irradiation room nearby laboratories, sharing geochronological and medical interests.

Currently, achieved energies of such devices are still below critical thresholds. Therefore, we used the ELBE linear accelerator facility at Dresden-Rossendorf (Helmholtz-Centre) in Germany. Even then, the possible maximum energy of 18 MeV at ELBE was still too low to expect J_{38}-values comparable to the neutron irradiation method (i.e., 10^{-4}–10^{-2}), which resulted in an experimentally quite challenging investigation. However, the energy still sufficed to study some basic properties of the ^{40}Ar/^{38}Ar method. Our investigation should be nonetheless regarded as a starting point only, since some key questions still need to be resolved by future studies at higher energy levels.

Theoretical framework of the ^{40}Ar/^{38}Ar method

Mitchell (1972) discussed most potential nuclear reactions involved with γ-ray irradiation. We report such reactions in Table 1 and, where available, list energy thresholds. Only limited new data have accumulated since.

Interaction modes of γ-rays with matter are highly energy dependent and are influenced by the nucleonic structure of the target atom, a discussion of which is beyond the scope of this study. The desired photon-induced reactions encompass an energy range of 5–35 MeV. Within this range, high-energy photons excite nuclear energy levels within the atom and may cause nucleon-nucleon oscillations. The latter is of

Table 1.
Overview of most important γ-induced reactions and their threshold energies with Ar, K and Ca isotopes

^{36}Ar production:		
	^{40}K (γ,α) ^{36}Cl (β$^-$, 300 ka) ^{36}Ar	**a[b] = 0.012% / threshold 6.43 MeV**
	^{40}Ca (γ,α) ^{36}Ar	**a = 96.94% / threshold 7.04 MeV**
^{37}Ar production:		
	^{39}K (γ,np) ^{37}Ar	a = 93.08% / threshold 18.2 MeV
^{38}Ar production:		
	^{39}K (γ,n) ^{38}K (β$^+$, 7.7 min) ^{38}Ar	**a = 93.08% / threshold 13.08 MeV**
	^{39}K (γ,p) ^{38}Ar	**a = 93.08% / threshold 6.37 MeV**
	^{40}Ar(γ,2n)^{38}Ar	**a = variable / threshold 16.2 MeV**
	^{40}K (γ,2n) ^{38}K (β$^+$, 7.7 min) ^{38}Ar	a = 0.012% / threshold 20.88 MeV
	^{41}K (γ,3n) ^{38}K (β$^+$, 7.7 min) ^{38}Ar	a = 6.91% / threshold not known
	^{42}Ca (γ,α) ^{38}Ar	**a = 0.64% / threshold 6.23 MeV**
	^{40}K (γ,np) ^{38}Ar	**a = 0.012% / threshold 14.16 MeV**
	^{40}Ca (γ,np) ^{38}K (β$^+$, 7.7 min) ^{38}Ar	a = 96.94% / threshold 21.42 MeV
^{39}Ar production:		
	^{40}K (γ,p) ^{39}Ar	**a = 0.012% / threshold 7.58 MeV**
	^{43}Ca (γ,α) ^{39}Ar	**a = 0.14% / threshold 7.58 MeV**
	^{41}K (γ,np) ^{39}Ar	a = 6.91% / threshold 17.67 MeV
^{40}Ar production:		
	^{41}K (γ,p) ^{40}Ar	**a = 6.91% / threshold 7.8 MeV**
	^{44}Ca (γ,α) ^{40}Ar	**a = 2.1% / threshold 8.84 MeV**
^{42}Ar production:		
	^{44}Ca (γ,2p) ^{42}Ar	a = 2.1% / threshold not known
	^{46}Ca(γ,α) ^{42}Ar	a = 0.004% / threshold not known

[a] Reactions notated in bold have thresholds significantly below our maximum energy of 17.6 MeV.
[b] Atomic abundance of respective isotope.

great importance because the cross section $\sigma_{total}(E_\gamma)$, which is a measure for a photon reaction, reveals broad maxima (several MeV width), in particular in the region of the Giant Dipole Resonance (GDR) (e.g., Balashov *et al.* 1961, Veyssière *et al.* 1974, Dietrich and Berman 1988, Kapitonov 2020) (Figure 1a–c for ^{39}K, ^{40}Ca and ^{40}Ar). Other multipole resonances commonly have lower reaction yields, but may contribute significantly. In addition, different kinds of product nucleons can be emitted. The most favoured reactions involve (γ,α) and (γ,n) reactions, the former occurring at lower threshold energies below 10 MeV (Hoffmann *et al.* 1966). The latter reaction is mostly associated with higher yields (e.g., Dietrich and Berman 1988), compared with (γ,2n) or (γ,3n) reactions that require higher energies and show lower yields. Photoproton reactions involve production of one or more protons. Such (γ,p) or (γ,np) reactions can be an important reaction path, showing significant contributions to the total photon cross section (e.g., Oikawa and Shoda 1977, O'Keefe *et al.* 1987, Van den Abeele *et al.* 1992). However two-proton reactions are energetically depressed as it is necessary to overcome the Coulomb barrier and commonly requires higher threshold energies compared with a photoneutron reaction. In detail, this strongly depends on the participating target and product nuclei, as the individual excitation states and availability of these differ for each atom.

In our study we exploit the reaction ^{39}K(γ,n)^{38}K(β$^+$, 7.7 min)^{38}Ar, the threshold energy of which is 13.08 MeV and the maximum cross section is about 15 mbarn at 18–22 MeV (Veyssière *et al.* 1974, Dietrich and Berman 1988). There are concurring reactions that are unwanted, in particular the reaction ^{40}Ca(γ,np)^{38}K(β$^+$, 7.7 min)^{38}Ar. The energy threshold of this reaction is higher, about 20.4 MeV (Veyssière *et al.* 1974, Dietrich and Berman 1988), and the ^{38}Ar-yield lower, but significant (about 10% relative contribution). Reactions involving ^{42}Ca or ^{43}Ca are negligible with respect to ^{40}Ca due to low cross sections and the low natural abundance of these isotopes. On the other hand, we benefit from some alternative reactions with K, which increase the ^{38}Ar-yield. For example, ^{38}Ar can be produced via the pathways ^{39}K(γ,p)^{38}Ar and ^{41}K(γ,3n)^{38}K (β$^+$, $t_{1/2}$ = 7.7 min)^{38}Ar. However, the latter requires a likely threshold energy of > 32 MeV (Dietrich and Berman 1988), and the former has a lower yield than the main photoneutron reaction, making both reactions probably negligible for geochronological purposes. ^{40}Ar is commonly present in larger amounts and thus, contributions from ^{44}Ca (γ,α)^{40}Ar are probably not significant. This might be different, however, if ages are low, and the observed ^{40}Ar/^{36}Ar ratios show only modest contributions of radiogenic ^{40}Ar*. In those cases, a correction could be more important. By far the larger

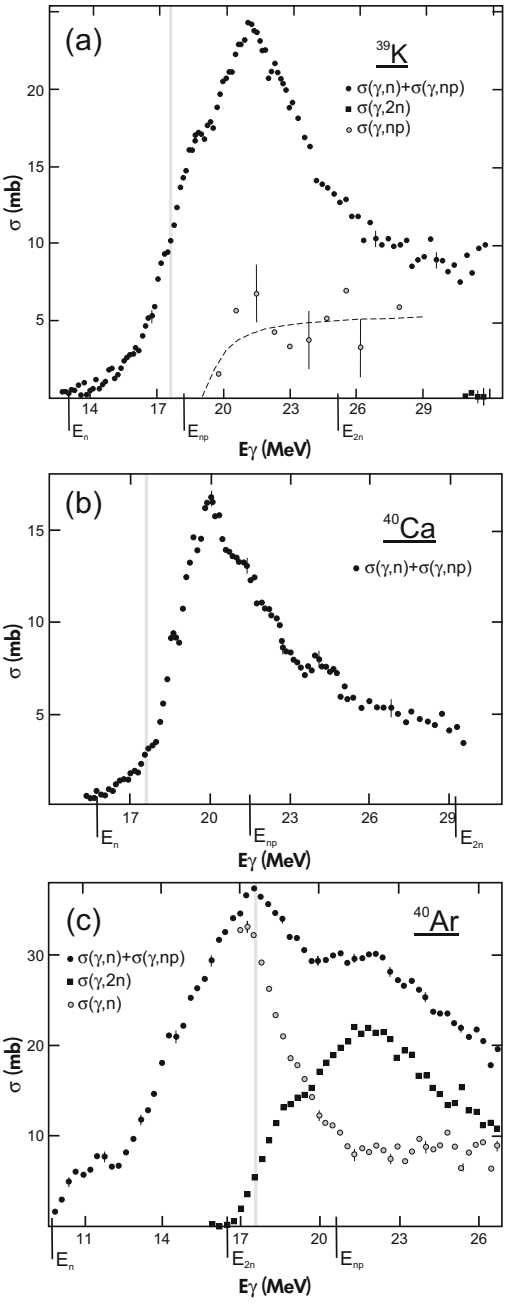

Figure 1. Cross section (in mb) versus γ-energies (in MeV) of reactions (a) ^{39}K(γ,n) and ^{39}K(γ,np), (b) ^{40}Ca(γ,n) + ^{40}Ca(γ,np) and (c) ^{40}Ar(γ,n), ^{40}Ar(γ,n) + ^{40}Ar(γ,np) and ^{40}Ar(γ,2n). Redrawn after Veyssière *et al.* (1974). Threshold energies E_i are marked at abscissa, subscript i denotes reaction product. Grey vertical line corresponds to maximum γ-energy available in our study.

problem arises from the reaction ^{40}Ca(γ,α)^{36}Ar, as the natural abundance of ^{40}Ca is much higher than for ^{44}Ca and ^{36}Ar much less abundant than ^{40}Ar. In addition, the threshold energies of both reactions are relatively low (about

7.04 and 8.84 MeV for ^{40}Ca and ^{44}Ca, respectively, Mitchell 1972) and contributions hard to avoid. In order to establish a robust dating method a way for correcting these interferences is mandatory. We propose that the reactions ^{44}Ca(γ,2p)^{42}Ar and/or ^{46}Ca(γ,α)^{42}Ar can be used for the interference corrections. There are no cross-sectional data available but in probability the necessary energy of the bremsstrahlung is above 25 MeV for the former reaction to supply enough ^{42}Ar, exceeding the maximum energy in this study of 17.6 MeV. The second reaction should occur at similar threshold energies as for other (γ,α) reactions, i.e., at ~ < 10 MeV. Hence, ^{42}Ar could have been produced in our experiment, but the low natural abundance of ^{46}Ca (0.004%) sets some limitations, which demands a higher sensitivity mass spectrometer. It is a future task to check these options in more detail. Expected production rates of $^{42}Ar_{Ca}$ are discussed in subsection "Feasibility considerations of the ^{40}Ar/^{38}Ar-method".

The ^{40}Ar/^{38}Ar-method ideally benefits from irradiation with high-energy γ-rays of up to 35 MeV. Commonly, γ-rays are produced as bremsstrahlung by accelerating electrons to the desired maximum energies and letting them hit a material with high nucleon number and good material strength. In our experiments, niobium was used as the target material. Unfortunately, the energy distribution of the created γ-rays was dominated by the lower energy photons whereas only a small portion approximated the maximum energy. Thus, with a maximum energy of 17.6 MeV we could only make use of about 1% of the total γ-ray flux to produce $^{38}Ar_K$, and only about 15% of the total cross section for $^{38}Ar_K$ production below ~ 32 MeV was covered (Figure 1a). Using the full range of the giant dipole resonance may result in yields by a factor of about 1000 times higher than available in this study. The electron flux in our experiment was about 1 mA, significantly higher than the 150 μA reported by Mitchell (1972) for his SLAC experiment. Eventually, the applied beam time directly influences the production rate. In comparison with the study of Mitchell (1972) our γ-irradiation lasted less than half the time.

Samples and experimental methods

Several age monitors (reference materials) commonly in use in the established ^{40}Ar/^{39}Ar method were selected for this study: HD-B1 bt (24.40 ± 0.09 Ma (1*s*), Schwarz and Trieloff 2007), GA1550 bt (99.86 ± 0.55 Ma (1*s*), Schwarz and Trieloff 2007), BMus2 (331.3 ± 1.1 Ma (1*s*), Schwarz and Trieloff 2007), MMhb (527.4 ± 2.6 Ma (1*s*), Samson and Alexander 1987), WA1ms (2613 ± 2.4 Ma (1*s*), Jourdan *et al.* 2014) and NL-25 hbl (2673 ± 4 Ma (1*s*), Schaeffer and Schaeffer 1977, Schwarz and Trieloff 2007). Given ages were recalculated with the decay constants according to the discussions in Renne *et al.* (2011) and Schwarz *et al.* (2011). We also included one muscovite from Swaziland (SW85-299, Sinceni pegmatite) with a reported Rb-Sr age of 3050 ± 25 Ma (1*s*) (Trumbull *et al.* 1993), recalculated with the ^{87}Rb decay constant of Villa *et al.* (2015) as 3110 ± 26 Ma (1*s*), as a possible 'internal' reference material. In addition, two GL-O glauconite reference materials in use for the traditional K-Ar method with a (recalculated) age of 96.0 ± 1.1 Ma (1*s*) (e.g., Odin *et al.* 1977, Clauer *et al.* 2005, Vandenberghe *et al.* 2014) and several CaF_2 reference materials were included in this study. We further irradiated two blank aluminium foils to check for contributions from the high-purity Al-foil used for packaging the samples. The respective compositions were atmospheric within 1*s* uncertainties (data not shown). We list all analysed monitors in online supporting information Appendix S1.

Furthermore, we investigated two whole rock samples of an illite-bearing Cambrian shale from Newfoundland, Canada (sample number 2012-00969, from Manuel River Formation, Drumium, stratigraphic age *ca.* 500.5–504.5 Ma, locality 47°31′30.5″N 52°57′04.6″W, stratigraphic height 14.37 m, collected by Gregor Austermann and Anne Hildebrand, Austermann *et al.* 2021). These shales show a low diagenetic overprint likely during the Ordovician with estimated temperatures for this location of about 200–250 °C (Austermann *et al.* 2021). The major K-phase in this shale is illite and has grain sizes of < 50 μm. Thus, it is a good candidate to investigate recoil-induced disturbances of the age spectrum, but also requires consideration of thermal processing.

We placed the samples in a cylindrical Al-container of 20 mm diameter, consisting of eight layers of 5 mm thickness with seven holes each. The sample notations "A" to "G" refer to respective positions with same letter corresponding to the same vertical sequence. The central hole "G" was surrounded by the other six positions and was slightly larger allowing for sample test portion masses up to 30 mg. Otherwise, masses were below 10 mg and adjusted to expected ^{40}Ar-signal heights. We determined all masses with a microgram-weighing device (last digit 0.1 μg). We sent this container to the linear accelerator facility ELBE at Dresden-Rossendorf, Germany. The maximum energy of the primary electron beam was 17.6 MeV. This primary beam hit a niobium plate inducing formation of bremsstrahlung, which is commonly used for physical experiments. The majority of electrons passed the target Nb and were soon after deflected into the electron beam dump consisting of a

graphite cylinder. This cylinder was mounted inside a water-cooled steel housing (maximum cooling power 50 kW, Schwengner *et al.* 2006). Compared with the main line a larger intensity of γ-rays was produced within this dump due to the larger dimension of the target. We placed our sample container in a tube line behind this electron beam dump. The orientation of this pipe was perpendicular to the direction of the electron beam and associated γ-rays. Hence, each sample layer plane within the container was aligned along the γ-ray beams. Irradiation time was 60 h; total luminescence of the primary beam was ~ 1 mA. For further information on the geometry of the linear accelerator hall and its basic instruments, refer to Schwengner *et al.* (2006).

After irradiation, the samples were placed in an ultrahigh vacuum line. Gas extraction was performed by heating in an inductively heated Mo-crucible at 1300 °C for 30 min. Only in the case of stepwise heating protocols (two HD-B1 biotite reference materials, both illite-bearing whole rocks and one GL-O reference material), and one more GL-O measured in a single extraction step, a resistance-heated furnace with a Ta-crucible was used. The respective heating time was 10 min for each temperature step, except for the single extraction step (30 min). We cleaned our sample gas with a cold and hot Zr-Al getter (400 °C) and a cold Ti-sponge-getter. In the case of the illite-bearing whole rock samples and the GL-O reference materials, we set the Ti sponge-getter to 650 °C. Common blank heights were about (0.7–1.1) × 10^{-8} cm^3 STP ^{40}Ar for 30 min heating time. The blank heights were higher than usual due to problems with the water-cooling system, which also restricted the maximum temperature to 1300 °C. A repeat analysis of all samples at 1300 °C indicated full gas extraction in the first degassing step, i.e., 1300 °C was sufficient for the samples included in this study. In spite of a higher blank, we could detect discernible excess $^{38}Ar_K$ in most samples and in fact, the biggest problem in the first instance was the low γ-ray energy and flux that resulted in a low J_{38}-value. This, however, was a result of this study and could not be significantly influenced beforehand.

We performed the analyses with an in-house modified VARIAN MAT CH5 noble gas mass spectrometer hosted at the Institut für Geowissenschaften, Heidelberg, Germany. All isotopes were detected with an electron multiplier in analogue mode with a wide dynamic range (common signal range was 1 pA to 1 μA) allowing for detection of isotope ratios of up to 1,000,000. We routinely controlled dependencies of isotope ratios and concentrations from gas amounts by analysing multiple and divided portions of our calibration gas. As ion source conditions we applied a 3 kV accelerating voltage and a trap current of 200 μA (first measurement series) and 290 μA (second measurement series), respectively. The maximum ionisation energy of the electron impact ionisation was 85 eV. In addition to the stable argon isotopes ^{36}Ar, ^{38}Ar and ^{40}Ar, we also monitored the radioactive isotopes ^{37}Ar (half-life = 35.1 d), ^{39}Ar (half-life = 269 a) and ^{42}Ar (half-life = 33 a). However, because of the low γ-ray energies and fluxes we expected no contribution from K or Ca on these masses and in fact observed no significant signals. Some minor observed signals (< 1 pA) are due to residual hydrocarbons (^{42}Ar mainly) and no systematic association with the Ca or K content of samples could be recognised. We report the blank corrected concentrations of these isotopes in Appendix S1. Note, that concentrations are partly exaggerated due to the low test portion masses.

Besides blank analyses, we bracketed the analyses by calibration gas measurements of air composition at beginning and closing of the day. In order to improve the precision of absolute concentrations our calibration gas content was cross-calibrated with the mean measured radiogenic ^{40}Ar content of 13 BMus2 analyses (expected 11.17 × 10^{-5} cm^3 STP g^{-1}, Schwarz and Trieloff 2007). The blanks before BMus2-analyses showed slightly elevated $^{40}Ar/^{36}Ar$-ratios in cases when another BMus2 age reference material was degassed prior at the same day. In opposite, blanks show no significant deviation from atmospheric composition in other reference materials when allowing for pumping overnight or longer (with two exceptions for which also another age reference material was measured prior at the same day, but with no impact on blank composition). We conclude that the elevated blanks are not a property of the furnace system but mirror an incomplete fixation at the charcoal held at liquid nitrogen temperature. However, the respective relative amounts are negligible to the amounts observed in the major standard extraction (below 0.83% $^{40}Ar_{Blank}/^{40}Ar^*$, see Appendix S1). Blank $^{38}Ar/^{36}Ar$-ratios were atmospheric within 2*s* uncertainties for forty-four out of forty-eight blank extractions, the remaining four extractions agree within 3*s* errors. For age evaluation, we considered the blank isotopic compositions as atmospheric and correction for blank is included in the overall correction for atmospheric argon. For this reason values for ^{36}Ar, ^{38}Ar, and ^{40}Ar are listed without blank correction in Appendix S1.

Ages were calculated with a decay parameter λ_{Total} = 5.5305 × 10^{-10} a^{-1} (Renne *et al.* 2011, Schwarz *et al.* 2011) and with atmospheric ratios of $^{40}Ar/^{36}Ar$ = 298.56 ± 0.31 and $^{38}Ar/^{36}Ar$ = 0.1885 ± 0.0006 (Lee *et al.* 2006).

Results

γ-ray flux distribution

We deduced the γ-ray flux distribution across the Al-container from the measured air-corrected $^{40}Ar^*/^{38}Ar_K$-ratio of our BMus2 muscovite reference material (monitor age 331.3 ± 1.1 Ma, Schwarz and Trieloff 2007, recalculated with ^{40}K decay parameters of Renne *et al.* 2011). This ratio varied from about 90,000 in layer 1 to about 50,000 in layer 8 (Figure 2, total length 4 cm). The flux was highest in the last two layers (7 and 8) and hardly differed from each other. This may indicate the beginning of a region of constant flux. The respective J_{38}-values ranged from (2.1–4.1) × 10^{-6}.

In three layers (4 to 6) we placed three BMus2-reference materials in order to recognise potential lateral variations (BMus2-6B analysis failed, however). Within uncertainties no gradient in γ-ray flux across individual ampoule layers was detected and hence, we averaged the respective J_{38}-values for each of these layers. This improved the precision of our step heating analyses of the illite-bearing rocks, which were intentionally placed in layers 4 and 5, respectively.

CaF_2 reference materials

In addition to the age monitors, we placed one CaF_2 reference material in each layer. Because of some technical problems, results for three CaF_2 reference materials were not reliable and are not included in this study. At applied maximum γ-ray energy of 17.6 MeV we expected a significant contribution of Ca-derived ^{36}Ar according to the reaction $^{40}Ca(\gamma,\alpha)^{36}Ar$. In fact, we observed lower-than-air $^{40}Ar/^{36}Ar$ ratios (Figure 3). As expected, the amount of Ca-derived ^{36}Ar increased from layer 1 to 8 according to the rising γ-ray flux from about 6 × 10^{-10} to 12.5 × 10^{-10} cm^3 STP g^{-1} (equivalent to conversion factors ConvCa = (1.3–2.5) × 10^{-9} cm^3 STP $^{36}Ar/[g \times g(Ca)]$). In addition, in a three-isotope diagram $^{40}Ar/^{36}Ar$ versus $^{38}Ar/^{36}Ar$ (Figure 3) the data (uncorrected for air) plot below a line through the origin and air composition. This implies a certain contribution of Ca-derived ^{38}Ar. We extrapolated mixing lines between air and data to $^{40}Ar/^{36}Ar = 0$ and calculated the mean of the respective *x*-axis intercept values that is equivalent to the production ratio $(^{38}Ar/^{36}Ar)_{Ca}$. We found a $(^{38}Ar/^{36}Ar)_{Ca}$ ratio of 0.07 ± 0.03 (1*s*). The precision of this value is relatively poor and we cannot rule out a systematic offset in ^{38}Ar. In addition, there may also be contributions to ^{40}Ar by the reaction $^{44}Ca(\gamma,\alpha)^{40}Ar$ (threshold energy 8.84 MeV). However, it seems unlikely that this reaction will affect the ^{40}Ar content significantly because the natural abundance of ^{44}Ca is only 2.1% and ^{40}Ar is much more abundant than ^{36}Ar.

For calculation of $^{40}Ar/^{38}Ar$ ages we used the calculated $(^{38}Ar/^{36}Ar)_{Ca}$ production ratio and the measured Ca-conversion factor to ^{36}Ar for correction of Ca-contributions by applying the nominal Ca-contents of respective reference materials (NL25 hb: 8.04 ± 0.01%,

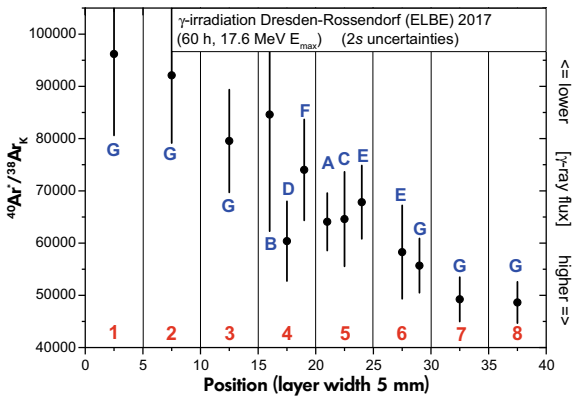

Figure 2. γ-ray flux distribution across capsule layers 1 to 8, indicated by measured $^{40}Ar^*/^{38}Ar_K$-ratios in BMus2 bt reference material. Capitals indicate positions in layer (see section "Samples and experimental methods"). Vertical bars on data points represent 2*s* uncertainties.

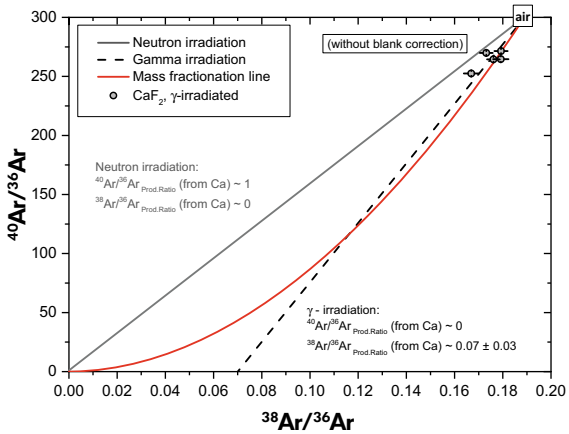

Figure 3. $^{40}Ar/^{36}Ar$ versus $^{38}Ar/^{36}Ar$ diagram for CaF_2-data. Lines indicate mixing trends of air composition and production rates (from neutron and γ-irradiation, respectively). Bars on data points are 1*s* uncertainties.

Schaeffer and Schaeffer 1977, MMhb: 7.44 ± 0.21%, Samson and Alexander 1987). This correction on ^{36}Ar was 0.7–1.3% for NL-25 and 1.2–2.0% for MMHb. The respective contribution of Ca-induced production of $^{36}Ar_{Ca}$ corresponded to (1.2–2.0) × 10^{-10} cm^3 STP g^{-1}.

Age reference materials

Our age monitors span a large age range from 24.4 Ma (HD-B1 bt) to 3110 Ma (SW85-299 ms). We display the calculated $^{40}Ar/^{38}Ar$-ages obtained by total fusion analyses and the nominal reference material ages in Figure 4 (1*s* uncertainties) and report these below with 2*s* uncertainties. The older reference materials show a clear deviation towards lower ages (Figure 4a), whereas the younger age monitors (i.e., below 1 Ga) show a reasonable 1:1 correlation (Figure 4b, c), though with relatively large uncertainties.

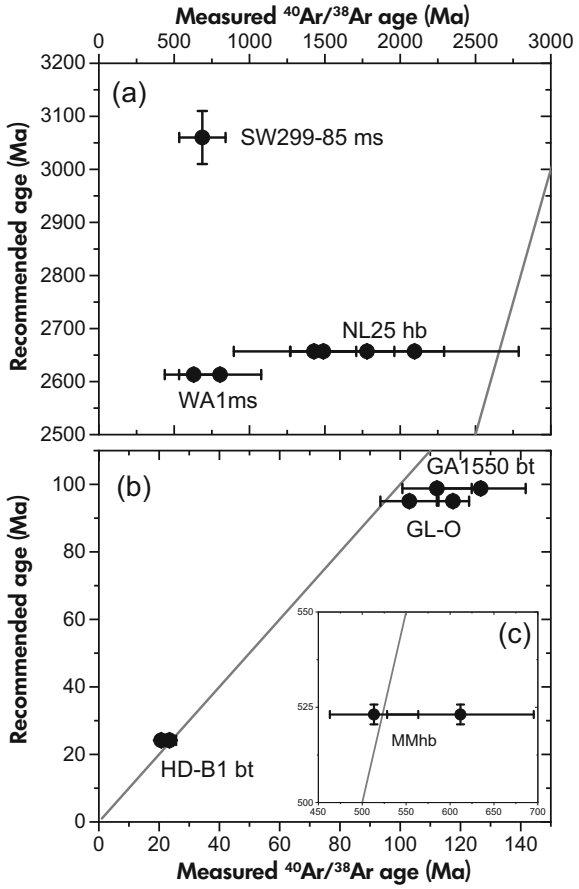

Figure 4. Comparison of expected and observed monitor ages. (a) Reference materials with ages > 1 Ga, (b) reference materials with ages below 100 Ma and (c) reference material MMhb. For younger monitors we observe a reasonable distribution along a line with slope = 1. Bars on data points represent 1*s* uncertainties.

Apparently, with a low J_{38}-value of the order of 10^{-6} we expect difficulties with old age reference materials. The calculated $^{40}Ar^*/^{38}Ar_K$-ratios in these reference materials nominally should be several hundreds of thousands to 1.5 million. Keeping the signal of $^{40}Ar^*$ in the order of the calibration gas signal (or, at most, few times above) was maintained by accordingly adjusting the masses of our reference samples. Hence, the masses of the high-K reference materials WAms1 (nominal age 2613 ± 4.8 Ma) and SW85-299 ms (nominal age 3110 ± 51 Ma) were only about 50 µg. In case of the NL25 hornblende reference material the lower K-content allowed for a higher mass (~ 5 mg) in spite of a similar nominal age (2673 ± 8 Ma) as the others. Even in the case of NL25 hornblende, and even more for the Precambrian muscovite samples, the expected $^{38}Ar/^{36}Ar$-ratios show only minor excess $^{38}Ar_K$ relative to the air-value. Such small amounts of K-derived ^{38}Ar are highly susceptible to disturbances. For example, even small contributions of hydrocarbons that survived the cleaning process may lead to an artificially enhanced $^{38}Ar/^{36}Ar$ ratio and hence, an overestimate of the $^{38}Ar_K$ content. As expected in such a case, the NL25 hbl ages of 1428 ± 1056 Ma to 2095 ± 1378 Ma are closer to its nominal age compared with the two Archaean muscovite samples for which we observed very erroneous ages of below 1 Ga (WA1ms: 805 ± 537 Ma / 629 ± 378 Ma, SW85-299 ms: 687 ± 304 Ma).

The younger age reference materials agree mostly, with the exception of one HD-B1 reference material, with their recalculated nominal ages within 2*s* uncertainties (GA1550 bt: 99.86 ± 1.1 Ma, GL-O: 96.0 ± 2.2 Ma, HD-B1 bt: 24.40 ± 0.18 Ma, and MMhb: 527.4 ± 5.2 Ma). The observed ages were GA1550 bt: 126.7 ± 29.8 Ma / 112.2 ± 23.0 Ma, GL-O: 103.1 ± 19.2 Ma, HD-B1 bt (total ages): 23.5 ± 2.1 Ma / 20.7 ± 2.0, and MMhb: 513 ± 100 Ma / 612 ± 167). This demonstrates the general viability of this method for geochronological purposes, as already shown by Mitchell (1972).

Results of stepheating analyses I – HD-B1 bt #3 and #4

We applied a stepwise heating protocol to the HD-B1 biotite reference materials #3 and #4 (24.40 ± 0.09 Ma, Schwarz and Trieloff 2007) (Figure 5). For this age reference

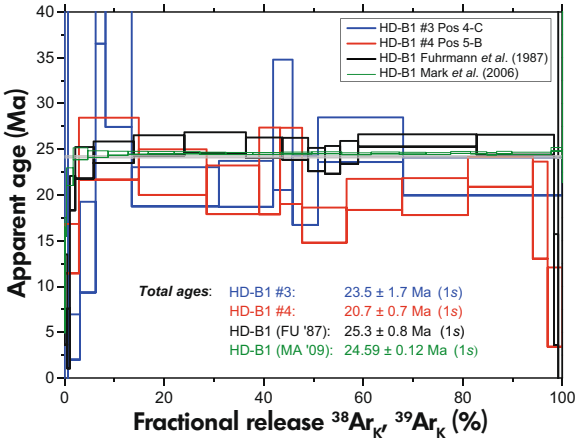

Figure 5. Ar age spectra for both HD-B1 bt samples and literature spectra obtained with the $^{40}Ar/^{39}Ar$-method (Fuhrmann *et al.* 1987, Mark *et al.* 2009). Note that we have not recalculated the ages of the latter with new decay constants. Uncertainties are 1*s*.

material, comparative $^{40}Ar/^{39}Ar$ spectra are available (Fuhrmann *et al.* 1987, Mark *et al.* 2009) that allow a comparison (Figure 5). Note that we have not recalculated the age data of these two studies with new decay constants, because here we are only interested in the general age pattern.

Both reference material aliquots showed nearly identical plateau patterns. The similarity also included a slightly lower apparent age at ~ 50% of the fractional gas release, though uncertainties are considerable. Interestingly, $^{40}Ar/^{39}Ar$ ages given by Fuhrmann *et al.* (1987) also mimic such a minor "dump" that might mirror thermal redistribution of Ar as a consequence of a differing diffusion behaviour of $^{40}Ar^*$ and $^{38}Ar_K$, $^{39}Ar_K$, respectively (Trieloff *et al.* 2005). However, Mark *et al.* (2009) observed no such variation. Their data show a very narrow perfect plateau spectrum at 24.59 ± 0.12 Ma (1*s*). Our $^{40}Ar/^{38}Ar$ ages tend to be lower than ages reported with neutron-irradiation, a feature that is nearly ubiquitous in this study, with only a few exceptions. We suggest this is a consequence of the observed rather small excess $^{38}Ar/^{36}Ar$ ratios and $^{38}Ar_K$ concentrations in our sample suite. This is even more relevant for a stepwise heating protocol.

Results of stepheating analyses II – GL-O #2

An important question related to the $^{40}Ar/^{38}Ar$ method is the problem of recoil redistribution of $^{38}Ar_K$ within a rock during the production process, analogous to the recoil process in neutron irradiation experiments observed for ^{39}Ar and ^{37}Ar. Such recoil will lead to complex age patterns in a stepwise heating analysis because K-rich sites may lose significant K-derived $^{38}Ar_K$ (or $^{39}Ar_K$ during neutron irradiation), which is either lost from the sample or replanted into K-poor neighbouring phases with a different degassing characteristic. The glauconite reference material GL-O is commonly used for conventional K-Ar dating and as such only reproducibility of the nominal total (recalculated) age of 96.0 ± 1.1 Ma is of importance. Hess and Lippolt (1986) studied it with the neutron-irradiation technique in a stepwise heating experiment, which allowed for a comparison of the observed age spectra. Glauconite is a secondary mineral formed during diagenesis from primary mica in soils. The respective maturation process naturally governs the age distribution within the glauconite. Because of its small grain size of about 200 ± 100 µm a notable recoil loss and redistribution could occur. In addition, thermal effects may influence the degassing scheme. For example, Hess and Lippolt (1986) observed a significant low-temperature degassing of ^{39}Ar and ^{40}Ar, in part already during the irradiation within the reactor (they used a glass capsule to catch the released argon during irradiation). Because reactor temperatures for neutron irradiation are typically 150–250 °C thermal effects appeared important. Note that temperatures during this γ-ray irradiation should be less, and probably below 50 °C, due to active cooling of the beam dump, but the exact temperature is unknown. We avoided heating the samples after placing them into the ultra-high vacuum extraction line, and instead pumped the line over several months. GL-O #1 had a lower mass and was degassed in one-step at 1300 °C. We obtained an age of 103.1 ± 9.6 Ma, in agreement with its nominal K-Ar age of 96.0 ± 1.1 Ma. In the case of the second aliquot (GL-O #2) we applied a stepwise heating procedure, and could largely reproduce the age pattern reported by Hess and Lippolt (1986). However, we observed no large low-temperature loss of $^{38}Ar_K$ comparable to the significant loss of $^{39}Ar_K$ found by Hess and Lippolt (1986). The maximum age of 133.1 ± 5.1 Ma in our study agrees with their maximum ages within error (Figure 6). Hess and Lippolt (1986) favoured a thermally-induced diffusional loss of argon as the cause for apparent ages below 96 Ma and large amounts of fractional ^{39}Ar-release at low temperatures. Because temperatures during γ-irradiation should have been much lower we would thus expect a different profile.

Peculiarly, our total age 117.5 ± 5.4 Ma derived from the step heating analysis differs from its nominal value and from the age observed for GL-O #1 by more than 2*s* uncertainties. It is unclear at present if this discrepancy is

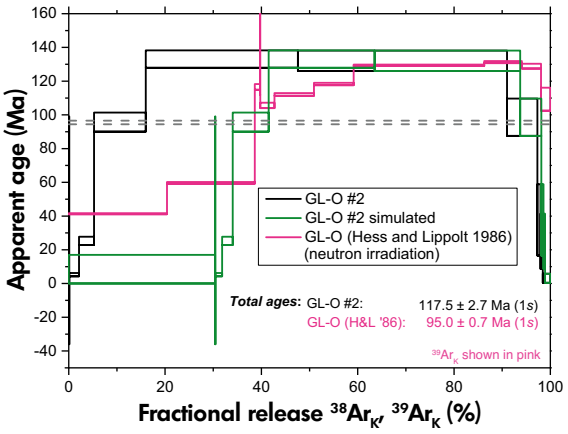

Figure 6. Ar age spectra for GL-O glauconite reference material and a literature spectrum obtained with the ^{39}Ar-^{40}Ar-method (Hess and Lippolt 1986). A simulated age spectrum with an assumed 30.4% loss of $^{38}Ar_K$ and 2.8% loss of radiogenic $^{40}Ar^*$ (equivalent with an age of 8.5 ± 8.5 Ma) before analyses is shown in green. Uncertainties are 1*s*.

purely statistical or if some $^{38}Ar_K$ was lost from the sample during the experiment by degassing overnight within a break or by recoil loss during irradiation. Both scenarios appear somewhat unlikely, because in the former case, ambient temperatures were low and, in case of the latter, because recoil loss should be not restricted to one glauconite split, but should affect both. A rough calculation demonstrates that about 30.4% $^{38}Ar_K$ is missing in GL-O #2 compared with GL-O #1. In addition, about 3% $^{40}Ar^*$ is missing relative to the expected concentration of 2.462×10^{-5} cm^3 STP (Clauer *et al.* 2005). We simulated a possible recoil loss of $^{38}Ar_K$ and thermal loss of radiogenic $^{40}Ar^*$ during irradiation by a rescaling of the fractional release in the age spectrum of GL-O #2, i.e., we assumed the total $^{38}Ar_K$ was 130.4% of the measured concentration (Figure 6, green spectrum). In addition, we set an apparent age of 8.5 ± 8.5 Ma in the modelled first extraction. As can be seen, the simulated age spectrum appears similar to the results of Hess and Lippolt (1986). This might point to a significant recoil loss of $^{38}Ar_K$ similar to the neutron irradiation technique (note that first extraction of Hess and Lippolt (1986) was emanated and collected into their ampoule).

From these results, we deduce a rather similar recoil problem of the $^{40}Ar/^{38}Ar$ method comparable to the neutron irradiation technique, but part of the problem with GL-O might also be related to thermal effects. A further check will require different grain size fractions of individual reference materials with known well-defined age spectra that we need to measure by both irradiation techniques, preferably at higher γ-energies and thus similar *J*-values for both irradiations.

Results of stepheating analyses III – Illite-bearing Cambrian black shale

We analysed two pieces of an illite-bearing Cambrian black shale from outcrops near Manuels River (Newfoundland, Canada) by a high-resolution stepwise heating approach. Again, the major host of K, illite, is present only in very small grain sizes (< 50 µm), but unlike GL-O not present as single grains. Thus, potential recoil will not necessarily lead to $^{38}Ar_K$-loss from the shale but rather to a redistribution within it. In the case of the first measured sample, illite #2, we chose temperature steps to derive a first impression of degassing characteristics and to check signal heights. Subsequently, we degassed sample #1 in higher-resolution temperature steps. Given the low *J*-value, our observed maximum $^{38}Ar/^{36}Ar$-ratios of 0.66 ± 0.10 (Illite #1) and 0.93 ± 0.12 (Illite #2) were rather large and may hint at hidden potential under more adequate irradiation conditions. Both analyses show a very similar age and degassing pattern (Figure 7). After young ages at the beginning, ages increased towards Cambrian ages at ~ 600–650 °C. At higher temperatures, again we observed a drop in age. We may assign the oldest age as a measure of the minimum true age of the rock. However, no 'plateau age' *sensu stricto* could be defined. Nonetheless, within error we could reproduce a realistic age, reflecting either the stratigraphic Cambrian age or, more likely, a documented Ordovician age of later diagenesis (Austermann *et al.* 2021). The younger ages at lower temperatures can be easily explained by partial argon loss, e.g., during diagenesis, weathering or due to a later thermal disturbance. The younger ages at higher temperatures might be caused by a recoil of $^{38}Ar_K$ from illite into more retentive low-K phases (e.g., plagioclase), but this remains speculative. Both observed total ages are Devonian ages and agree within their 1*s* uncertainties (#1: 375.8 ± 21.7 Ma; #2: 395.2 ± 15.2 Ma).

Results of stepheating analyses IV – Isochron calculations

In a similar way to the $^{40}Ar/^{39}Ar$ method, it is possible to plot data in isochron diagrams of type $^{40}Ar/^{36}Ar$ *vs.* $^{38}Ar/^{36}Ar$ (normal) and $^{36}Ar/^{40}Ar$ *vs.* $^{38}Ar/^{40}Ar$ (inverse). Unlike the $^{40}Ar/^{39}Ar$ method, we observed a positive slope

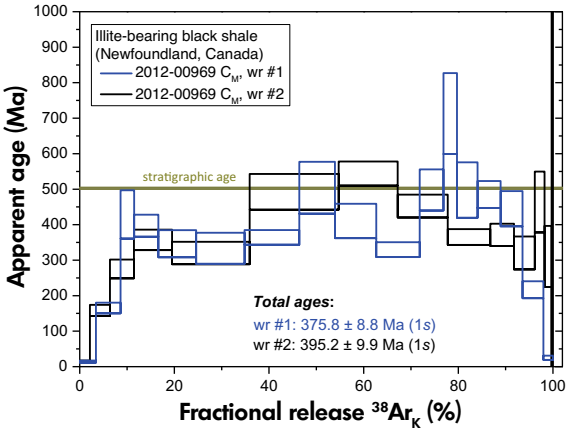

Figure 7. Ar age spectra for two illite-bearing Cambrian black shale aliquots from Newfoundland, Canada. Both samples agree well within error in shape of their age pattern and their total ages. Maximum ages agree with their stratigraphic age, pointing to incomplete reset of the K-Ar system during diagenesis (age of Cambrian after Ogg *et al.* 2016). Uncertainties are 1*s*.

for the inverse method, which is a direct consequence of a non-zero initial (trapped) $^{38}Ar/^{40}Ar$-ratio. In contrast, the trapped $^{39}Ar/^{40}Ar$-ratio would be zero for the neutron-irradiation method. The slope of an inverse isochron corresponds to $\{(^{36}Ar/^{40}Ar)-(^{36}Ar/^{40}Ar)_{TRAPPED}\}$ / $\{(^{38}Ar/^{40}Ar)-(^{38}Ar/^{40}Ar)_{TRAPPED}\}$. Because for all reasonable cases we can assume that the numerator is positive, a negative slope would solely depend on the $(^{38}Ar/^{40}Ar)$ ratios, i.e., a negative denominator results in a negative slope. Since we also can set $^{38}Ar/^{40}Ar = (e^{\lambda t}-1)/J$, the slope of the inverse isochron depends on the *J*-value of the γ-irradiation and age of the sample. At a given age we need to choose a *J*-value of sufficient height to get a negative slope (and vice versa). The respective boundary condition for a negative slope is $J > (e^{\lambda t}-1)/\left(\frac{^{40}Ar}{^{38}Ar}\right)_{Trapped}$. At *J*-values $>10^{-3}$ the respective crossover age would be ~13.3 Ga, i.e., we would commonly expect negative slopes for reasonable irradiation fluxes.

For all samples, we calculated isochrons with error-correlation (Figure 8a–j). The statistical weight of regressions (MSWD, *p*-value) with IsoplotR (Vermeesch 2018) were relatively poor, due to the large uncertainties of our data, with the exception of HD-B1 #4. Inverse and normal isochron ages of the HD-B1 bt agree with each other and with the nominal reference material age within 2*s* uncertainties (Appendix S1, Figure 8a–d). Both isochron ages of the GL-O reference material agree (136.3 ± 3.5 Ma and 135.4 ± 5.2 Ma, Figure 8e, f) and are equivalent with the observed maximum age of 133.1 ± 5.1 Ma. Finally, both isochron ages of shale sample #1 (Figure 8g, h) are identical (369 ± 33 Ma and 363 ± 99 Ma) and correspond with its total $^{40}Ar/^{38}Ar$ age of 375.8 ± 8.8 Ma. The second split #2 yielded Cambrian ages within error for gas extractions 400–1000 °C (N = 12) (551 ± 33 Ma and 536 ± 64 Ma, Figure 8i, j). This could be merely a statistical artefact, because if all fourteen extractions are included in a normal isochron regression, we obtain a lower age of 464 ± 16 Ma. However, the Cambrian age could also indicate low natural thermal processing of this shale and a low irradiation induced recoil redistribution within the sample.

To summarise, all isochron ages agree with observed maximum ages (GL-O #2 and illite #2) or total ages (HD-B1 bt and illite #1) demonstrating the internal consistency of the $^{40}Ar/^{38}Ar$ systematics.

Discussion

Our results demonstrate that the $^{40}Ar/^{38}Ar$ technique delivers reasonable geochronological results – at least if the *J*-value is appropriate to the sample age. Since future applications require a higher γ-ray energy and flux, it makes sense to discuss some additional nuclear reactions that would highly promote the application of this method. First, we will review our current results.

Feasibility considerations of the $^{40}Ar/^{38}Ar$ method

A geochronologist is mainly interested in high precision ages and in a method that can be applied to a large set of rocks, which are in this case K-bearing. Our results show that even with difficult boundary conditions (i.e., low γ-ray flux with suited energy, relatively high blank levels) we can obtain reasonable ages with 'internal precisions' (i.e., without errors of age reference materials and decay constant) of about 10%. This is of course far above the precision that can be achieved with the $^{40}Ar/^{39}Ar$-method (permil-range). In our study, amounts of ^{38}Ar were low and a precision of the ^{38}Ar-signal better than 1.5% could be achieved only rarely. However, this can be easily compensated with 100–1000 times higher γ-ray fluxes. Mitchell (1972) reported a *J*-value of about 1.4×10^{-4}, though the electron current of the SLAC was one order of magnitude lower than ours (but with twice the irradiation time and a higher energy threshold of 35 MeV). In essence, his yield was a factor of 11 larger

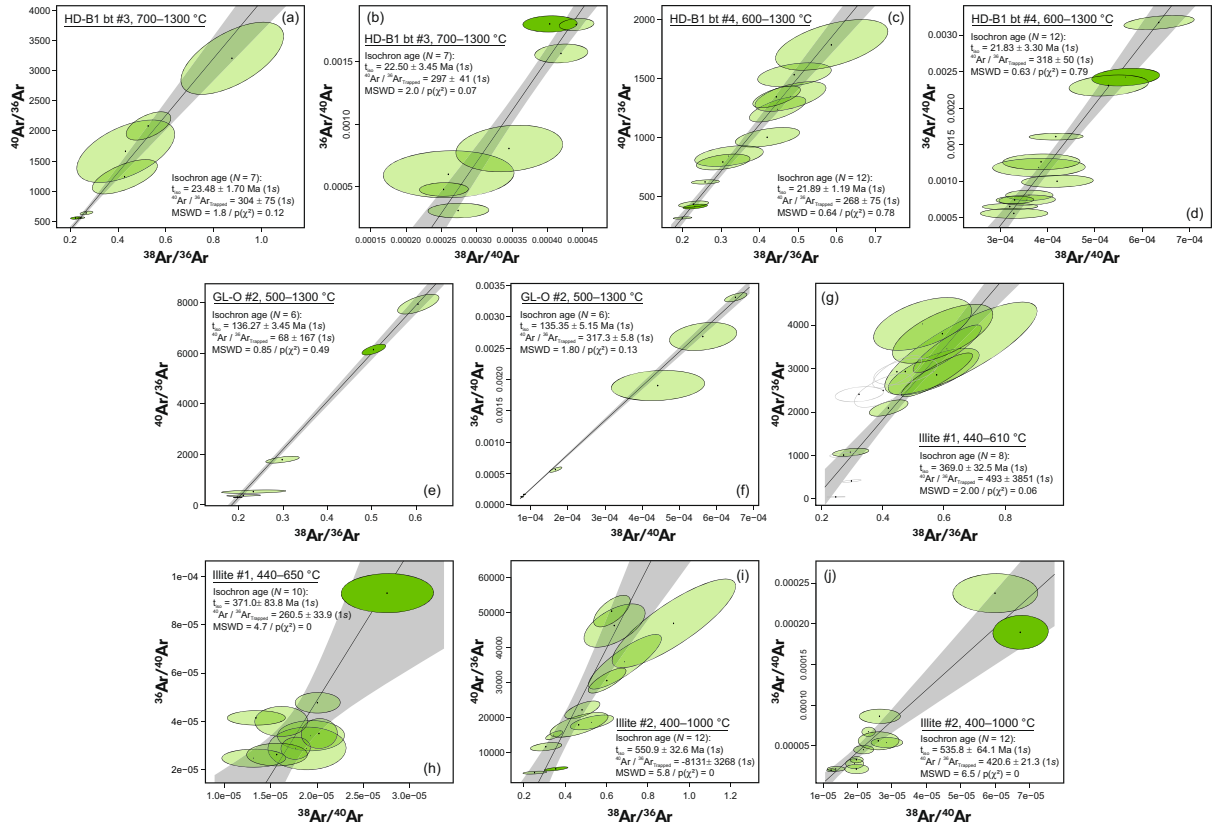

Figure 8. Examples of normal and inverse isochrons for (a, b) HD-B1 bt #3, (c, d) HD-B1 bt #4, (e, f) GL-O #2, (g, h) Illite #1 and (i, j) Illite #2, respectively. Calculation with error correlation was performed with IsoplotR (Vermeesch 2018). Ellipses represent 1*s* uncertainties.

compared with our experiment. However, we have only used a rather small proportion of γ-rays with an energy range suitable for producing $^{38}Ar_K$ (about 1%), covering only ~ 15% of the total cross section (Figure 1a), and using a rather small irradiation time of 60 h. The latter two would already account for a factor of 20. The rise in proportion of reacting γ-rays is more difficult to quantify, because it depends also on geometry and target properties. A lower estimate from bremsstrahlung spectra adds another factor of 20 (expanded energy range of interest factor 7, expected minimum increase in contributing average photons/MeV ~ factor of 3) resulting in a 400 times higher flux. A 1000 times higher flux would result in $^{38}Ar/^{36}Ar$-ratios of 200–700 and $(^{40}Ar/^{38}Ar)_K$-ratios of 50–90 for our BMus2 age reference material and about 750–1500 for the older age monitors. Apparently, the precision of ^{38}Ar concentration data and $(^{40}Ar/^{38}Ar)_K$ ratios would be similar to the $^{40}Ar/^{39}Ar$ method.

A major source of trouble is the unavoidable deconvolution of interfering isotopes produced by reactions with Ca. In addition, we need to calculate the trapped argon composition in order to recognise potential deviations from atmospheric compositions. Others had outlined the principles of this evaluation process for the $^{40}Ar/^{39}Ar$-method in vast details (a summary can be found in McDougall and Harrison 1999). However, in $^{40}Ar/^{38}Ar$-dating we must face two important differences. Firstly, ^{38}Ar potentially consists of three components, K-derived, Ca-derived and a trapped component. The latter is also associated with ^{36}Ar. In addition, we proved the existence of Ca-derived ^{36}Ar. Because the terrestrial $^{38}Ar/^{36}Ar$-ratio of 0.1885 is constant (Kunz 1999, Lee *et al.* 2006), a correction for ^{36}Ar can be easily implemented. However, we first need to deconvolve the Ca-derived fractions of ^{36}Ar and ^{38}Ar. A correction of Ca-derived $^{38}Ar_{Ca}$ in an analogous way as for the neutron-based method requires another argon isotope without further interferences except from Ca. We propose that one possible way to achieve this is production of ^{42}Ar (half-life 33a) from reactions (1) $^{44}Ca(\gamma,2p)^{42}Ar$ and (2) $^{46}Ca(\gamma,\alpha)^{42}Ar$. No literature data about cross-sections of these particular reactions are available. However, cross-sectional

data on photoreactions with ^{44}Ca in general suggest a small cross-section for reaction (1) (Harty and Thompson 1981). These authors showed that the total photoneutron cross-section (i.e., (γ,n), (γ,2n) and (γ,np) reactions) is relatively large (up to 60 mbarn), whereas the (γ,p) reaction is much less likely (up to 1.5 mbarn at 21 MeV, Harty and Thompson 1981). However, (γ,2p) reactions should be even more depressed because it is more difficult to release two charged particles from the atom due to the Coulomb barrier. In essence, we would require a high *J*-value and higher γ-energies to produce ^{42}Ar in substantial amounts by reaction (1). For example, we may assume a 1000 times lower cross section for reaction (1) compared with production of $^{38}Ar_K$ by a (γ,n) reaction. This estimate might be supported by photoactivation data obtained at 60 MeV bremsstrahlung by Kato *et al.* (1976) who report yields of different reaction branches depending on proton number *Z*. Our observed maximum conversion factor for K is convK = 2.8×10^{-8} cm^3 STP $^{38}Ar_K$ STP/(g × g[K]), with the target ^{39}K being the major isotope of K (93.08%). ^{44}Ca has an abundance of 2.1% and hence, the total conversion factor convCa with ^{42}Ar would be about 50,000 times lower, about 5.5×10^{-13} cm^3 STP/(g × g[Ca]). This is calculated for the experimental settings of our current study. Production of ^{42}Ar in our CaF_2 reference materials would thus correspond to about 10^{-15} cm^3 STP (calculated for 5 mg). However, a 100–1000 times higher *J*-value seems possible and, thus, the concentration of ^{42}Ar may reach low, but measurable values of up to 10^{-12} cm^3 STP / (5 mg). Nothing is reported about the threshold energy for reaction (1) to occur. An arrow mark in figure 8 of Dular *et al.* (1959/60) denoting the threshold energy of (γ,2p) reactions for natural Ca indicates a threshold energy of 14.8 MeV, but it is unclear from which source this value is derived and whether this threshold is also valid for ^{44}Ca (it is probably linked to ^{40}Ca). The maximum yield of such a reaction would be probably observed above 20 MeV, however. Reaction (2) utilises ^{46}Ca as target isotope, which has a low natural abundance of 0.00004. The reaction threshold might be similarly low to other, known Ca(γ,α)Ar reactions (below 10 MeV). Assuming a similar production ratio of ^{42}Ar from ^{46}Ca as for ^{36}Ar from ^{40}Ca, we estimate an expected maximum concentration of $(5–10) \times 10^{-14}$ cm^3 STP $^{42}Ar_{Ca}$ g^{-1} in our CaF_2 experiments. This would correspond to an absolute ^{42}Ar concentration of max. 2.5×10^{-16} cm^3 STP (for 5 mg CaF_2), which is far below the detection limit of the CH5 mass spectrometer. Because of the low energy threshold, we should have observed the peak production rate. Only an increase in irradiation time and photon flux would raise this rate further. The latter would be automatically enlarged to a certain extent by the changing bremsstrahlung spectra with elevating the maximum γ-energies because of the increasing amount of photons in the medium energy range below 10 MeV. However, the impact appears modest (probably less than a factor of 10).

To our current knowledge ^{42}Ar is only produced by reactions with Ca isotopes in relevant portions and as such even small amounts that are detectable via ion counting techniques in modern high-sensitivity mass spectrometers might give a measure of Ca (estimated few thousand counts per second). This needs to be tested in a future study.

Recoil by γ-ray reactions

Recoil causes a distinct displacement length of the product nucleus during a nuclear reaction. Because this displacement is dependent on the transferred energy and subsequent collisions with other atoms of various masses, recoil lengths may vary. Commonly, we regard the mean of these lengths deduced from a large number of atoms as the effective recoil length and only this will be treated here. As with neutron-irradiation in ^{40}Ar/^{39}Ar dating this displacement can cause tremendous difficulties in obtaining ages of fine-grained materials. The recoil lengths of ^{39}Ar (from ^{39}K) and ^{37}Ar (from ^{40}Ca) in the neutron-irradiation technique are about 0.1 μm and 0.3 μm, respectively (Turner and Cadogan 1974, Villa 1997, Jourdan *et al.* 2007). We would also expect some recoil for argon isotopes produced by γ-irradiation. To glean information about recoil lengths after γ-irradiation requires consulting quite old studies. Van Lint *et al.* (1961) determined the mean energy-dependent recoil lengths for Cu, Ag and Au in the energy range of 11 to 26 MeV. Though with considerable scatter the (corrected) recoil lengths were 60–230 Å (Cu), 30-100 Å (Ag) and 20 Å (Au), as expected decreasing with atomic mass and increasing with energy (except for gold, for which no significant variation was observed). Since K and Ca have lower atomic masses than Cu we expect a somewhat larger recoil length, probably in the range of 300–400 Å at 26 MeV. However, note that van Lint *et al.* (1961) discussed pure substances, not mixtures of elements with various atomic masses. Most rocks of interest for geochronological applications contain dominantly lighter elements compared with K or Ca, e.g., O, Si, Mg and Al. The only heavier major element is Fe. We thus would expect a certain reduction of this recoil length by collisions with these lighter elements, to which momentum is transferred. Therefore, based on these data from van Lint *et al.* (1961) we consider 400 Å as the upper limit. Compared with the neutron-induced recoil lengths this would be about three to ten times less. Unfortunately, the age pattern of our shale sample does not provide enough precision to reliably estimate recoil

effects. At lower temperatures, we should observe anomalous old ages due to loss of $^{38}Ar_K$. However, this might be more than counterbalanced by loss of $^{40}Ar^*$, probably in the course of weathering or during diagenesis. At medium temperatures, we observe a kind of "age plateau" of Cambrian age, but no substructure could be resolved. A final decrease of ages at elevated temperatures might be evidence of recoil redistribution into phases with lower K-contents. The stepwise heating analysis of the glauconite K-Ar reference material GL-O also does not provide safe evidence for or against significantly different recoil effects. As discussed previously, our age spectrum nearly perfectly fits the only stepwise heating spectrum obtained with the $^{40}Ar/^{39}Ar$-method (Hess and Lippolt 1986). These authors attribute the peculiar pattern with low ages at lower temperatures to thermally induced diffusion-related processes. The only difference with our measurement is the by far larger release of K-related ^{39}Ar at low temperatures and ages below its K-Ar age of 96.0 Ma (5.5% $^{38}Ar_K$ versus 38.6% $^{39}Ar_K$). Because Hess and Lippolt (1986) could analyse the whole argon budget this might indicate that our $^{38}Ar_K$ concentration (from γ-irradiation) suffered a recoil-induced loss (see subsection "Results of stepwise heating experiments – GL-O #2"). However, thermal effects might also play an important role, as suggested by Hess and Lippolt (1986), demanding future studies to finally resolve the recoil problem.

Alternative dating approach: The $^{40}Ar/^{37}Ar$ method

Looking at the reaction schemes (Table 1) we can recognise that ^{37}Ar is produced from ^{39}K by a (γ,np) reaction. The energy threshold is 18.2 MeV and thus above the maximum energy in this study. Hence, we could not check for production rates of this reaction. Because ^{37}Ar is unstable (half-life 35.1 d) analyses need to be done quickly after irradiation. However, if this can be accomplished this would enable correction for interference reactions, in particular of Ca on ^{36}Ar. We expect no significant Ca-derived ^{37}Ar (the cross-section and energy threshold of reaction $^{40}Ca(\gamma,npp)^{37}Ar$ are unlikely to favour ^{37}Ar-production). With Ca-free age reference materials (the most common case) a $(^{37}Ar/^{38}Ar)_K$ production rate can be calculated, since there will be sufficient $^{38}Ar_K$. From this we can correct the total ^{38}Ar in a sample for its K-derived contribution and obtain a mixture of Ca-derived and trapped ^{38}Ar. The same applies to ^{36}Ar. Because the trapped terrestrial $^{38}Ar/^{36}Ar$-ratio can be assumed to be constant, we may apply the lever rule for a two-component mixture to finally compute the trapped ^{36}Ar necessary to correct for the trapped ^{40}Ar contribution (and for some minute contributions from Ca on ^{40}Ar), enabling the construction of isochrons. The most important caveat with this approach is the decay correction of ^{37}Ar. We need to know precisely the start and end times of irradiation, and the time spent until analysis to keep systematic uncertainties as small as possible. This can be quantified as follows: a systematic deviation of 2 h (e.g., because of wrongly cross-calibrated clocks) would introduce a systematic relative error of the J_{37}-value of 0.16%.

As a side aspect, dating of Ca-free minerals should be possible with both methods, utilising $^{37}Ar_K$ and $^{38}Ar_K$. Hence, we can extract two ages from one measurement, which should coincide (as long as no unexpected major differences in recoil behaviour prevail). This would clearly improve precision and accuracy of respective apparent ages.

Extension to extra-terrestrial samples

Extra-terrestrial samples, i.e., meteorites or sample-return specimen, are fragments of larger meteorite parent bodies that once were attached to an even larger asteroidal or planetary object. Commonly, these objects are detached from near the surface (a few metres) of its parent meteoroid or planetary body, and as such they are susceptible to interaction with galactic and solar cosmic rays (GCR and SCR) on a time-scale of several millions of years. The major component of these cosmic rays is high energetic γ-rays, which cause fragmentation of nuclides and production of secondary energetic particles (neutrons, protons, pions, myons) that may induce a cascade of follow-up reactions. During this process both ^{36}Ar and ^{38}Ar are produced by spallation reactions with mainly Ca, Fe and Ni, changing the $^{36}Ar/^{38}Ar$-composition in meteorites. In order to deconvolve the spallogenic and trapped ^{36}Ar and ^{38}Ar, respectively, we can make use of the independently determined spallation production ratio of $^{36}Ar/^{38}Ar = 0.65 \pm 0.02$ (e.g., derived from analyses of iron meteorites, Lämmerzahl and Zähringer 1966). The energies of the cosmic γ-rays exceed the maximum range of our bremsstrahlung energies by far, with solar cosmic rays having energies of several 100 MeV (but low penetration depth) and galactic cosmic-rays commonly showing energies above 1 GeV. Therefore, production rates of cosmic ray produced Ar isotopes differ from values obtained by irradiation with lower energy photons.

Apparently, because both argon isotopes suffer from additional interference reactions with Ca-nuclides, a

correction for these remains mandatory. Hence, it appears that application of the γ-Ar-Ar dating method to extra-terrestrial rocks relies on the production of ^{42}Ar and ^{46}Ca. Commonly, Ca contents of chondrites are about 1% *m/m* and typical test portion amounts are 50 mg. With a calculated convCa = 5.5×10^{-13} cm^3 STP $^{42}Ar/(g \times g$ [Ca]) (see subsection "Feasibility considerations of the ^{38}Ar-^{40}Ar method") this would correspond to an absolute concentration of 2.75×10^{-16} cm^3 STP ^{42}Ar. Assuming, an absolute ^{42}Ar amount of 1×10^{-12} cm^3 STP is necessary for detection, the production rate should be ~4000 times larger. This value could be up to a factor 10 lower if we account for some additional production due to longer irradiation time and a higher share of reacting γ-rays (see subsection "Feasibility considerations of the $^{40}Ar/^{38}Ar$-method"). Nonetheless, dating of extra-terrestrial material will push this method to its limits and first requires robust knowledge of ^{42}Ar-production rates from Ca and a more precise knowledge of Ca-interference parameters. Application to meteorite chronology is probably not the first step in developing this method further, unless the Ca-correction (i.e., $(^{36}Ar/^{38}Ar)_{Ca}$) is at the lower error bound determined in this study.

Conclusions

The $^{40}Ar/^{38}Ar$ dating method utilises irradiation with γ-rays and exploits the reaction $^{39}K(\gamma,n)^{38}K(\beta^+, t_{1/2} = 7.7$ min$)^{38}Ar$ to extract geochronological information, and resembles the established $^{40}Ar/^{39}Ar$ dating method that is based on irradiation with fast neutrons. Our investigation of some basic properties of this technique demonstrate the general feasibility of this method, even though the maximum achieved energy of the γ-ray bremsstrahlung of 17.6 MeV was limited to the lower end of necessary energies. We expect higher necessary energies to increase the production rate of $^{38}Ar_K$ and associated *J*-values to about 2–3 orders of magnitude. In spite of these restrictions and a large γ-ray flux gradient ($^{40}Ar^*/^{38}Ar_K$-ratios ranged from 48,600 to 96,200) analyses of commonly used Ar-Ar reference materials of younger ages (< 1 Ga) showed reasonable agreement with reported ages, demonstrating the reliability of the method. Deviations, in particular for older age monitors, are not a consequence of a principle failure of the technique, but a result of the low achieved production rate within this study. We confirm the predicted production of Ca-derived $^{36}Ar_{Ca}$ via reaction $^{40}Ca(\gamma,\alpha)^{36}Ar$ by analyses of co-irradiated CaF_2 reference materials with a production rate of $(1.3–2.5) \times 10^{-9} cm^3$ STP $^{36}Ar_{Ca}/(g \times g$[Ca]). More importantly, we observed production of $^{38}Ar_{Ca}$ with an estimated production ratio of $(^{38}Ar/^{36}Ar)_{Ca} = 0.07 \pm 0.03$ (1*s*). This ratio is expected to increase with higher irradiation energies and clearly would confine routine applications to Ca-poor K-minerals.

Results of our analyses of fine-grained samples show no particular difference to analyses with the neutron irradiation technique and, hence, we conclude that recoil redistribution might be similar or only slightly improved compared with the classical Ar-Ar method. However, a final judgement requires irradiation with higher energies, because thermal effects might be superimposed.

Isochron calculations were restricted by the relatively low precision but otherwise work similarly to the classical case of the $^{40}Ar/^{39}Ar$ method.

We conclude that the γ-irradiation technique is a viable alternative to the neutron irradiation Ar-Ar dating technique. The most problematic issue remains resolving the interference reactions from Ca, if it is intended to analyse Ca-bearing samples. We propose the reactions $^{44}Ca(\gamma,2p)^{42}Ar$ and $^{46}Ca(\gamma,\alpha)^{42}Ar$ could supply enough signal for analysis at high *J*-values, even though the first reaction is strongly suppressed due to the involved Coulomb-barrier, and the second reaction involves a target isotope with low natural abundance. In addition, the first reaction probably requires higher energies (probably > 25 MeV) to provide reasonable yields. Alternatively, short-lived ^{37}Ar is also expected to be produced via ^{39}K $(\gamma,np)^{37}Ar$ with a threshold of 18.2 MeV. As no interference reactions from Ca-isotopes on ^{37}Ar are expected, we may introduce another dating tool – the $^{40}Ar/^{37}Ar$ γ-ray technique. Remaining interferences from Ca could be corrected via ^{36}Ar-^{38}Ar relations. In spite of having a short half-life of 35.1 d, utilising ^{37}Ar could expand applications to terrestrial Ca-bearing rocks. Dating of extra-terrestrial samples with cosmogenic Ar contributions on top of contributions from Ca and trapped Ar still requires an independent measure of Ca-interferences, i.e., $^{42}Ar_{Ca}$.

It will still be some time until the $^{40}Ar/^{38}Ar$-technique can concur with the $^{40}Ar/^{39}Ar$-method, which profits from a 50-year database and experience. However, several issues make the γ-technique interesting if all the problematic issues are resolved. There is still higher potential in dating fine-grained samples (e.g., clay minerals, unequilibrated meteorites) compared with the neutron-irradiation technique. With simultaneous application of two chronological tools ($^{40}Ar/^{37}Ar$, $^{40}Ar/^{38}Ar$) precision and accuracy may still rise. Furthermore, locally installed irradiation facilities make sample handling easier and there is full control of the irradiation schedule.

Acknowledgements

The authors are grateful to funding by the Klaus-Tschira-Stiftung gGmbH. We acknowledge handling and coordinating the irradiation experiment at the ELBE facility of the Helmholtz-Centre in Dresden-Rossendorf by and helpful comments from R. Schwengner. We thank two anonymous reviewers who clearly improved this manuscript. Open Access funding enabled and organized by Projekt DEAL.

Data availability statement

The data that support the findings of this study are available in the supplementary material of this article (online supporting information).

References

Austermann G., Kling M., Ifrim C., Emondt P.D. and Hildenbrand A. (2021)
Quantifying the diagenetic impact in the late Ediacaran and Early Palaeozoic of the Avalon Peninsula using illite "crystallinity". **Canadian Journal of Earth Sciences**, **58**, 1187–1208.

Balashov V.V., Shevchenko V.G. and Yudin N.P. (1961)
Two-body forces and the giant resonance in photonuclear reactions. **Nuclear Physics**, **27**, 323–336.

Clauer N., Huggett J.M. and Hillier S. (2005)
How reliable is the K-Ar glauconite chronometer? A case study of Eocene sediments from the Isle of Wight. **Clay Minerals**, **40**, 167–176.

Dietrich S. and Berman B.L. (1988)
Atlas of photoneutron cross sections obtained with monoenergetic photons. **Atomic Data and Nuclear Data**, **38**, 199–338.

Dular J., Kernel G., Kregar M., Mihailović M.V., Pregl G., Rosina M. and Zupančič Č. (1959/60)
Nuclear absorption of gamma rays in Al, Si, P, S and Ca. **Nuclear Physics**, **14**, 131–139.

Fuhrmann U., Lippolt H.J. and Hess J.C. (1987)
Examination of some proposed K-Ar standards: $^{40}Ar/^{39}Ar$ analyses and conventional K-Ar data. **Chemical Geology**, **66**, 41–51.

Harty P.D. and Thompson M.N. (1981)
The photoneutron cross section of ^{44}Ca. **Australian Journal of Physics**, **34**, 505–510.

Hess J.C. and Lippolt H.J. (1986)
Kinetics of Ar isotopes during neutron irradiation: ^{39}Ar loss from minerals as a source of error in $^{40}Ar/^{39}Ar$ dating. **Chemical Geology**, **59**, 223–236.

Hogmalm K.J., Zack T., Karlsson A.K.-O., Sjöqvist A.S.L. and Garbe-Schönberg D. (2017)
In situ Rb-Sr and K-Ca dating by LA-ICP-MS/MS: An evaluation of N_2O and SF_6 as reaction gases. **Journal of Analytical Atomic Spectrometry**, **32**, 305–313.

Jourdan F., Frew A., Joly A., Mayers C. and Evans N.J. (2014)
WA1ms: A ~ 2.61 Ga muscovite standard for $^{40}Ar/^{39}Ar$ dating. **Geochimica et Cosmochimica Acta**, **141**, 113–126.

Jourdan F., Matzel J.P. and Renne P.R. (2007)
^{39}Ar and ^{37}Ar recoil loss during neutron irradiation of sanidine and plagioclase. **Geochimica et Cosmochimica Acta**, **71**, 2791–2808.

Jourdan F. and Renne P.R. (2013)
Neutron-induced ^{37}Ar recoil ejection in Ca-rich minerals and implications for $^{40}Ar/^{39}Ar$ dating. **In Jourdan F., Mark D.F. and Verati C. (eds), Advances in $^{40}Ar/^{39}Ar$ dating: From archaeology to planetary sciences. Geological Society of London, Special Publication, 378**, 33–52.

Kapitonov I.M. (2020)
Giant dipole resonance of nuclei with the number of nucleons 12–65. **Moscow University Physics Bulletin**, **75**, 181–191.

Kato T. and Masumoto K., Sato N., Suzuki N. (1976)
The yields of photonuclear reactions for multielement photon-activation analysis. **Journal of Radioanalytical Chemistry**, **32**, 51–70.

Kunz J. (1999)
Is there solar argon in the Earth's mantle? **Nature**, **399**, 649–650.

Lämmerzahl P. and Zähringer J. (1966)
K-Ar-Altersbestimmungen an Eisenmeteoriten – II Spallogenes Ar^{40} und Ar^{40}-Ar^{38}-Bestrahlungsalter. **Geochimica et Cosmochimica Acta**, **30**, 1059–1074.

Lee J.-Y., Marti K., Severinghaus J.P., Kawamura K., Yoo H.-S., Lee J.B. and Kim J.S. (2006)
A redetermination of the isotopic abundances of atmospheric argon. **Geochimica et Cosmochimica Acta**, **70**, 4507–4512.

Mark D.F., Barfod D., Stuart F.M. and Imlach J. (2009)
The ARGUS multicollector noble gas mass spectrometer: Performance for $^{40}Ar/^{39}Ar$ geochronology. **Geochemistry Geophysics Geosystems**, **10**, https://doi.org/10.1029/2009GC002643.

McDougall I. and Harrison T.M. (1999)
Geochronology and thermochronology by the $^{40}Ar/^{39}Ar$ method (2nd edition). **Oxford University Press (Oxford)**, 269pp.

references

Merrihue C.M. and Turner G. (1966)
Potassium-argon dating by activation with fast neutrons. Journal of Geophysical Research, 71, 2852–2857.

Mitchell J.G. (1972)
Potassium-argon dating of gamma-irradiated minerals. Earth and Planetary Science Letters, 14, 91–96.

Odin G.S., Velde B. and Bonhomme M. (1977)
Radiogenic argon in glauconites as a function of mineral recrystallization. Earth and Planetary Science Letters, 37, 154–158.

Ogg J.G., Ogg G. and Gradstein F.M. (2016)
A concise geologic time scale. Elsevier, 240pp.

Oikawa S. and Shoda K. (1977)
Photoprotons from ^{44}Ca, ^{45}Sc and ^{46}Ti. Nuclear Physics A277, 301–316.

O'Keefe G.J., Thompson M.N., Assafiri Y.I. and Pywell R.E. (1987)
The photonuclear cross sections of ^{48}Ca. Nuclear Physics A469, 239–252.

Paine J.H., Nomade S. and Renne P.R. (2006)
Quantification of ^{39}Ar recoil ejection from GA1550 biotite during neutron irradiation as a function of grain dimensions. Geochimica et Cosmochimica Acta, 70, 1507–1517.

Renne P.R., Balco G., Ludwig K.R., Mundil R. and Min K. (2011) Response to the comment by W.H. Schwarz *et al.* on "Joint determination on ^{40}K decay constants and ^{40}Ar*/^{40}K for the Fish Canyon sanidine standard, and improved accuracy for ^{40}Ar/^{39}Ar geochronology" by P.R. Renne *et al.* (2010). Geochimica et Cosmochimica Acta, 75, 5097–5100.

Samson S.D. and Alexander Jr. E.C. (1987)
Calibration of the interlaboratory ^{40}Ar/^{39}Ar dating standard MMHb-1. Chemical Geology, 66, 27–34.

Schaeffer G.A. and Schaeffer O.A. (1977)
^{39}Ar-^{40}Ar ages of lunar rocks. Proceedings of the 8th Lunar Planetary Science Conference, 2253–2300.

Schwarz W.H. and Trieloff M. (2007)
Intercalibration of ^{40}Ar-^{39}Ar age standards NL-25, HB3gr hornblende, GA1550, SB-3, HD-B1 biotite and BMus/2 muscovite. Chemical Geology, 242, 218–231.

Schwarz W.H., Kossert K., Trieloff M. and Hopp J. (2011)
Comment on the "Joint determination on ^{40}K decay constants and ^{40}Ar*/^{40}K for the Fish Canyon sanidine standard, and improved accuracy for ^{40}Ar/^{39}Ar geochronology" by Paul R. Renne *et al.* (2010). Geochimica et Cosmochimica Acta, 75, 5094–5096.

Schwengner R., Beyer R., Dönau R., Grosse E., Hartmann A., Junghans A.R., Mallion S., Rusev G., Schilling K.D., Schulze W. and Wagner A. (2005)
The photon-scattering facility at the superconducting electron accelerator ELBE. Nuclear Instruments and Methods in Physics Research A, 555, 211–219.

Trieloff M., Falter M., Buikin A.I., Korochantseva E.V., Jessberger E.K. and Altherr R. (2005)
Argon isotope fractionation induced by stepwise heating. Geochimica et Cosmochimica Acta, 69, 1253–1264.

Trumbull R.B. (1993)
A petrological and Rb-Sr isotopic study of an early Archean fertile granite-pegmatite system: The Sinceni pluton in Swaziland. Precambrian Research, 61, 89–116.

Turner G. and Cadogan P. (1974)
Possible effects of ^{39}Ar recoil in ^{40}Ar-^{39}Ar dating. Proceedings of the 5th Lunar Planetary Science Conference, 1601–1615.

Van den Abeele C., Ryckbosch D., Ryckbosch J., Dias J., Van Hoorebeke L., Van de Vyver R., Adler J.-O., Andersson B.-E., Isaksson L., Ruijter H. and Schröder B. (1992)
High-resolution ^{40}Ca(γ,p) measurements and the photoproton reaction mechanism. Physics Letters B, 296, 302–306.

Vandenberghe N., Harris W.B., Wampler J.M., Houthuys R., Louwye S., Adriaens R., Vos K., Lanckacker T., Matthijs J., Deckers J., Verhaegen J., Laga P., Westerhoff W. and Munsterman D. (2014)
The implications of K-Ar glauconite dating of the Diest Formation on the palaeogeography of the Upper Miocene in Belgium. Geologica Belgica, 17, 161–174.

Van Lint V.A.J., Schmitt R.A. and Suffredini C.S. (1961)
Range of 2–60-keV recoil atoms in Cu, Ag, and Au. Physical Reviews, 121, 1457–1463.

Vermeesch P. (2018)
IsoplotR: A free and open toolbox for geochronology. Geoscience Frontiers, 9, 1479–1493.

Veyssière A., Beil H., Bergère R., Carlos P., Leprêtre A. and De Miniac A. (1974)
A study of the photoneutron contribution to the Giant Dipole Resonance of s-d shell nuclei. Nuclear Physics, A227, 513–540.

Villa I.M. (1997)
Direct determination of ^{39}Ar recoil distance. Geochimica et Cosmochimica Acta, 61, 689–691.

Villa I.M., De Bièvre P., Holden N.E. and Renne P.R. (2015)
IUPAC-IUGS recommendation on the half life of ^{87}Rb. Geochimica et Cosmochimica Acta, 164, 382–385.

Supporting information

The following supporting information may be found in the online version of this article:

Appendix S1. Measurement results and age evaluations, blank data, reference materials, sample measurement results and uncorrected data.

This material is available from: http://onlinelibrary.wiley.com/doi/10.1111/ggr.12489/abstract (This link will take you to the article abstract).